Status of Progress Towards Acoustic Magnetized Target Fusion at General Fusion

D. Richardson, A. Froese, V. Suponitsky, M. Reynolds, D. Plant
General Fusion Inc., 108-3680 Bonneville Place, Burnaby, BC V3N 4T5 (www.generalfusion.com)
doug@generalfusion.com

Abstract

Magnetized Target Fusion (MTF) is a hybrid approach to fusion in which a self-organized plasma is compressed with the inertia of a conductive liner to conditions that fulfill the Lawson criterion [1]. This paper provides an overview of MTF and the ongoing research at General Fusion (GF) to design, test, and demonstrate the ability to produce energy using its acoustic MTF technology.

1. Introduction and Background

Magnetized Target Fusion was first proposed in the 1970's as a low-cost approach to fusion that combines the advantages of magnetic confinement fusion and inertial confinement fusion by working in an intermediate regime of plasma density and confinement time. The U.S. Naval Research Laboratory did pioneering work on one of the early MTF concepts with the LINUS program [2], which was unique among MTF schemes by employing a liquid metal liner to address the traditional fusion challenges of heat extraction, tritium breeding, and neutron flux on structural components [3,4]. The liquid liner made the compression inherently repeatable, but at the time could not be accelerated to sufficiently high velocities to compress plasma within its thermal lifetime. General Fusion is pursuing an acoustically-driven MTF concept that makes use of modern servo controllers which precisely time piston impacts to create an acoustic wave in the liquid metal liner. This wave will compress the target plasma in less than 200 μs, similar to the practically achievable plasma lifetimes in modern self-organized plasma devices. An MTF reactor with the potential to achieve net gain can be developed given current technologies.

In General Fusion's design, the deuterium-tritium fuel is supplied as a pair of magnetized plasma rings, known as compact toroids (CT). The CTs are delivered to an evacuated vortex inside a volume of liquid lead-lithium eutectic (atomic percentage ratio 83% Pb, 17% Li; hereafter referred to as Pb-17Li) for the duration of an acoustically-driven spherical collapse. The cavity volume is reduced by three orders of magnitude, raising the plasma density from 10^{17} ions/cm^3 to 10^{20} ions/cm^3, the temperature from 0.1 keV to 10 keV, and the magnetic field strength from 2 T to 200 T. The fusion energy will be generated during the 10 μs that the plasma spends at maximum compression, after which the compressed plasma bubble causes the liquid metal wall to rebound. Most energy is liberated as neutron radiation that directly heats the liquid metal. Using existing industrial liquid metal pumping technology the heated liquid metal is pumped out into a heat exchange system, thermally driving a turbine generator. The cooled liquid metal is pumped back into the vessel tangentially to reform the evacuated cylindrical vortex along the vertical axis of the sphere. Liquid Pb-17Li is ideal as a liner because it has a low melting point, low vapor pressure, breeds tritium, has a high mass for a long inertial dwell time, and has a good acoustic impedance match to steel, which is important for efficiently generating the acoustic pulse. The 100 MJ acoustic pulse is generated mechanically by hundreds of pneumatically-

driven pistons striking the outer surface of the reactor sphere. The acoustic pulse propagates radially inwards, strengthened by geometric focusing from 1 GPa to 10 GPa at the surface of the vortex.

Acceleration of compact toroids (CTs) is a synthesis of two well-developed concepts: the spheromak plasma configuration and the railgun accelerator. A compact toroid is a self-organized spheromak plasma containing embedded toroidal and poloidal magnetic fields, which decays principally by resistive dissipation of the plasma currents over several hundred microseconds. A railgun switches stored electrical energy from a capacitor bank into two rails with a moving projectile acting as an armature providing a conduction path between the rails. This creates a variable-inductance line with expanding stored magnetic flux pushing the projectile and accelerating it. A CT accelerator differs from a railgun by replacing the armature-projectile with a compact toroid, which can then be accelerated to speeds in excess of 100 km/s. The CT accelerators in General Fusion's design are located at the poles of the evacuated vortex. The injected CTs travel to the center of the sphere and merge to form a stationary compressible plasma target. The plasma ions are ohmically heated during merging by magnetic reconnection.

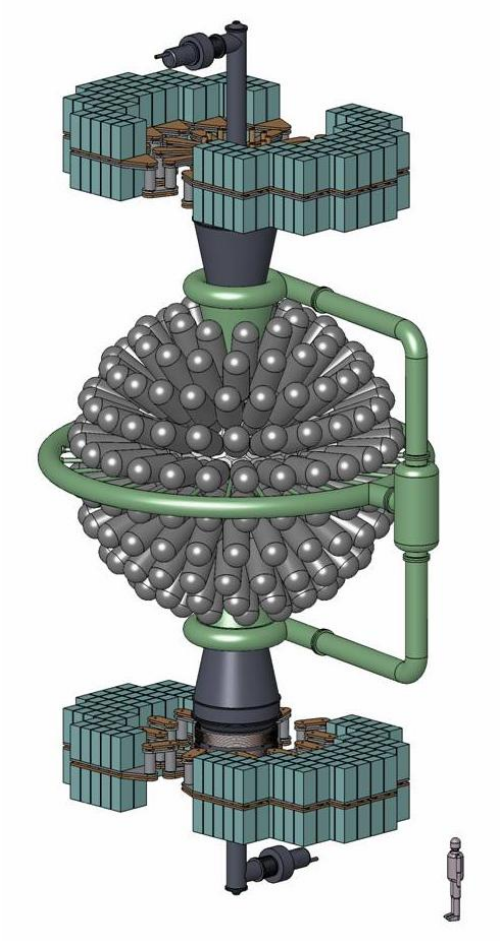

Figure 1: General Fusion's Acoustic Magnetized Target Fusion Reactor Concept

For a future power plant, economics, neutronics, tritium supply, and reactor energy density need to be considered. The eutectic absorbs the bulk of the fusion products through elastic scattering and provides a straightforward means of extracting the energy. The thick blanket significantly shields the wall by reducing the neutron flux on the structure and by lowering the neutron energy spectrum [5]. The 4 pi coverage provides an enhanced tritium breeding ratio (TBR) of 1.6 to 1.8 [6]. The neutron multiplication factor results from the Pb(n,2n) reaction and also from the $^{7}Li + n \rightarrow {}^{4}He + {}^{3}H + n$ reaction as diagrammed by Moyer [7]. The challenge with a thick Pb-17Li liner is likely to be too much tritium production.

This paper summarizes General Fusion's activities during 2012 to prove the viability of its MTF technology. Efforts are focused on mitigating risks and testing full scale components for acoustically-driven compression of plasma in the proposed reactor, in order to validate the predicted plasma behavior and demonstrate net gain. The MTF program is divided into the following areas: Acoustics Driver, Plasma Injector, and in support of these, Numerical Simulation.

2. Progress on Acoustic Driver

The acoustic driver consists of a 100 kg, 300 mm diameter, hammer that is accelerated down a one meter long bore by compressed air. The hammer's position is measured as it traverses the bore and its speed is controlled by an electronic braking system. This control system directs the hammer to impact a stationary anvil at a precisely controlled time. The collision generates a well timed acoustic pulse that can then be coupled into liquid metal.

A recently constructed test stand for developing and improving the acoustic driver is shown in Figure 2. During the last year, 850 shots were made on this test stand including 39 shots with 50 m/s impact speed.

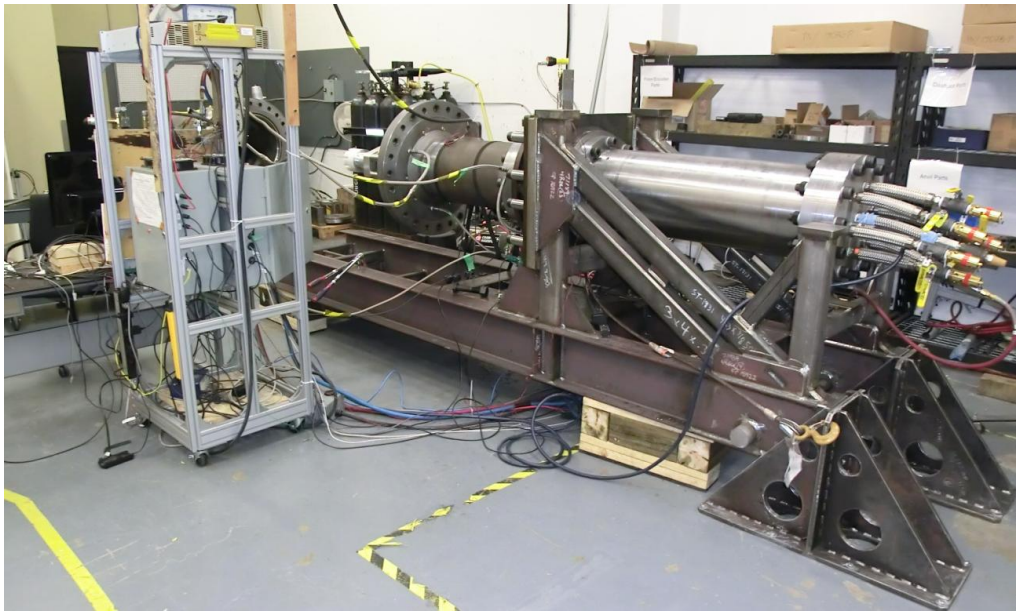

Figure 2: 'HP3b' acoustic driver test stand. The grey acoustic driver can be seen on the left hand side, while the large silver tube on the right, is an energy absorbing device used in place of liquid metal.

The best high speed timing performance recorded a sequence of 4 consecutive shots, at 50 m/s impact velocity, arrive within 2 us of the target time. The steady improvement in the acoustic driver's performance is a result of improved control system signal processing and hammer launching hardware. Work is ongoing to improve the system's shot to shot repeatability.

Testing is also progressing to find suitable materials for both the hammer and anvil assemblies. So far four materials have been identified as candidates; Bohler-Uddeholm 'Dievar', QuestTek 'Ferrium M54', Carpenter 'AerMet 100', and Vascomax 'C300'.

Although the applied loads are similar, the material requirements for the anvils and the hammers are slightly different. The anvils will be in continuous contact with molten metal, so they need to operate at elevated temperatures. Whereas, the hammers don't operate at high temperatures, but they do have complex features machined into them, making them susceptible to failures originating from geometric stress concentrations. Dievar is currently under test as both a hammer and an anvil material. A full sized Dievar anvil, installed in the HP3b test rig, has seen 38 impacts at 50 m/s, as well as hundreds of

low speed impacts. The part, so far, shows no sign of failure running at room temperature. Elevated temperature testing of the Dievar material was carried out on the Mini-Piston test rig shown in Figure 3.

Figure 3: Mini-piston, in horizontal position, without lead tank installed. This machine, which is a 1/3rd scale version of General Fusion's full scale pistons uses an air- actuated hammer in a bore that impacts a stationary anvil. A molten lead tank can be fitted onto this device to study both the pressure wave propagation in the liquid metal as well as the behavior of materials when they exposed to liquid metals under high loads.

Two samples of small Dievar anvils were tested on this machine with impact speeds of 50 m/s – 55 m/s. In total, 13 tests were run on these samples with impact speeds at, or over, 50 m/s. For a given impact speed, the stresses in the small anvils are expected to closely mimic the stresses in the full size anvils. The tests were done at elevated temperature and the anvil faces were in direct contact with molten lead. Although no evidence of cracking was found in these test pieces, as seen in Figure 4, significant pitting was observed on the lead interface surface. It is thought that this is likely due to cavitation.

The Mini-Sphere, shown in Figure 5 was commissioned with various combinations of drivers during which pressures and strains in the system were measured. The goal of this program was to validate the structural models of the sphere's various components and evaluate the mechanical integrity of the device. Several deficiencies were identified and now design improvements are being implemented.

After the sphere's commissioning was complete, ten shots were made with the full complement of 14 pistons firing under servo control. These shots had impact velocities ranging from 7 m/s to 10 m/s.
The resulting vortex collapses were filmed using a high speed camera and the imagery was compared to the results of CFD simulations. Figure 6 shows the progression of the vortex wall collapse as the pressure waves converge. The wall of the vortex turns to a spray soon after the arrival of the pressure wave. This effect is thought to be from a combination of Richtmyer–Meshkov instabilities (RMI) on

the vortex surface and a poorly formed cavitation region in the lead, generated by pressure pulse reflection very close to the vortex wall. Work continues to both improve the error in arrival time spread, and to increase the impact velocity. The current goal is to achieve an impact timing error spread of +/- 10us with a impact speed of 20 m/s. Work also continues to understand and control the spray that is generated during the collapse of the vortex.

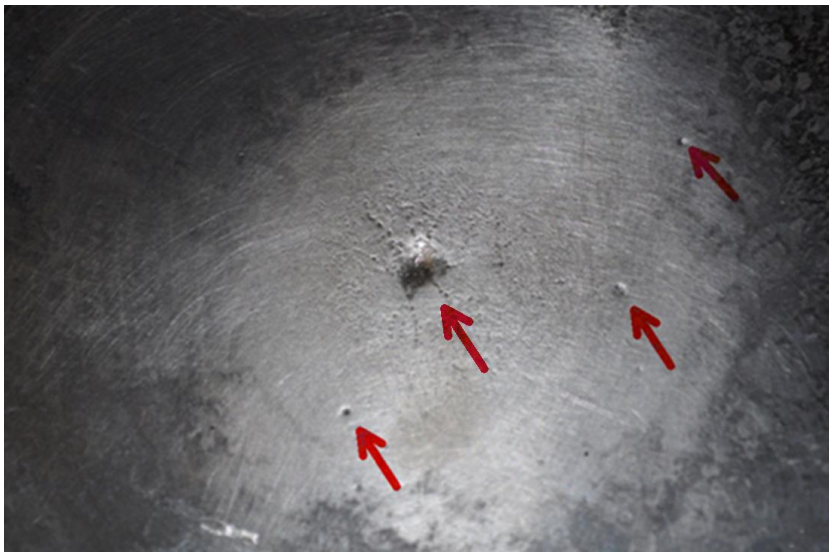

Figure 4: Pitting on liquid lead exposed anvil face after several 50 m/s impacts.

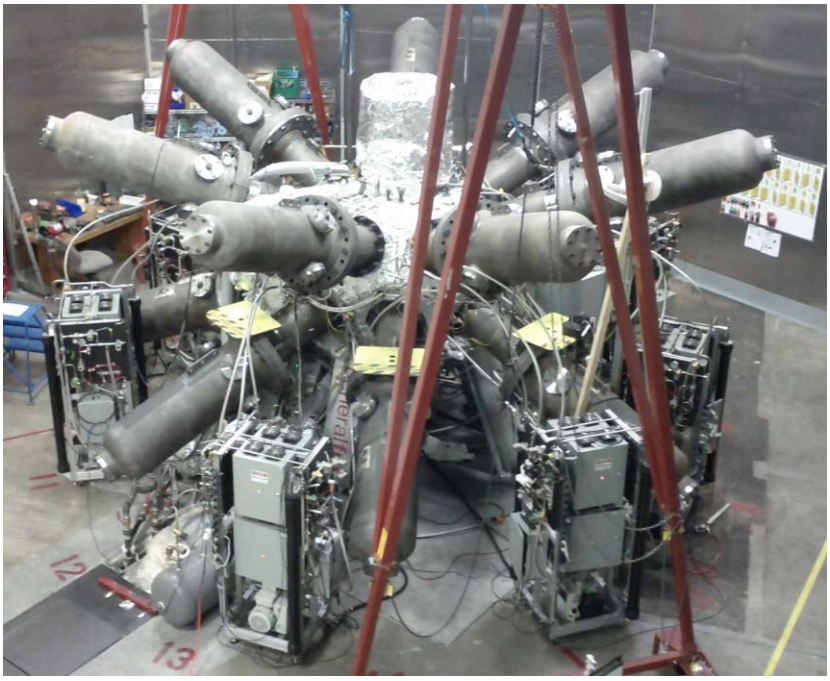

Figure 5: Mini-Sphere, a 1 meter spherical, liquid lead filled, tank with acoustic drivers mounted around the exterior, has 14 drivers, arranged in two rings of 7 drivers each. The hammers impact anvils that are in direct contact with the liquid lead, imparting pressure pulses into the molten metal. Lead is pumped around the inside of the sphere, creating a cylindrical vortex in the centre of the device. The inner wall of the vortex can then be imaged as pressure waves, travelling in from the radial pistons, converge and collapse the vortex

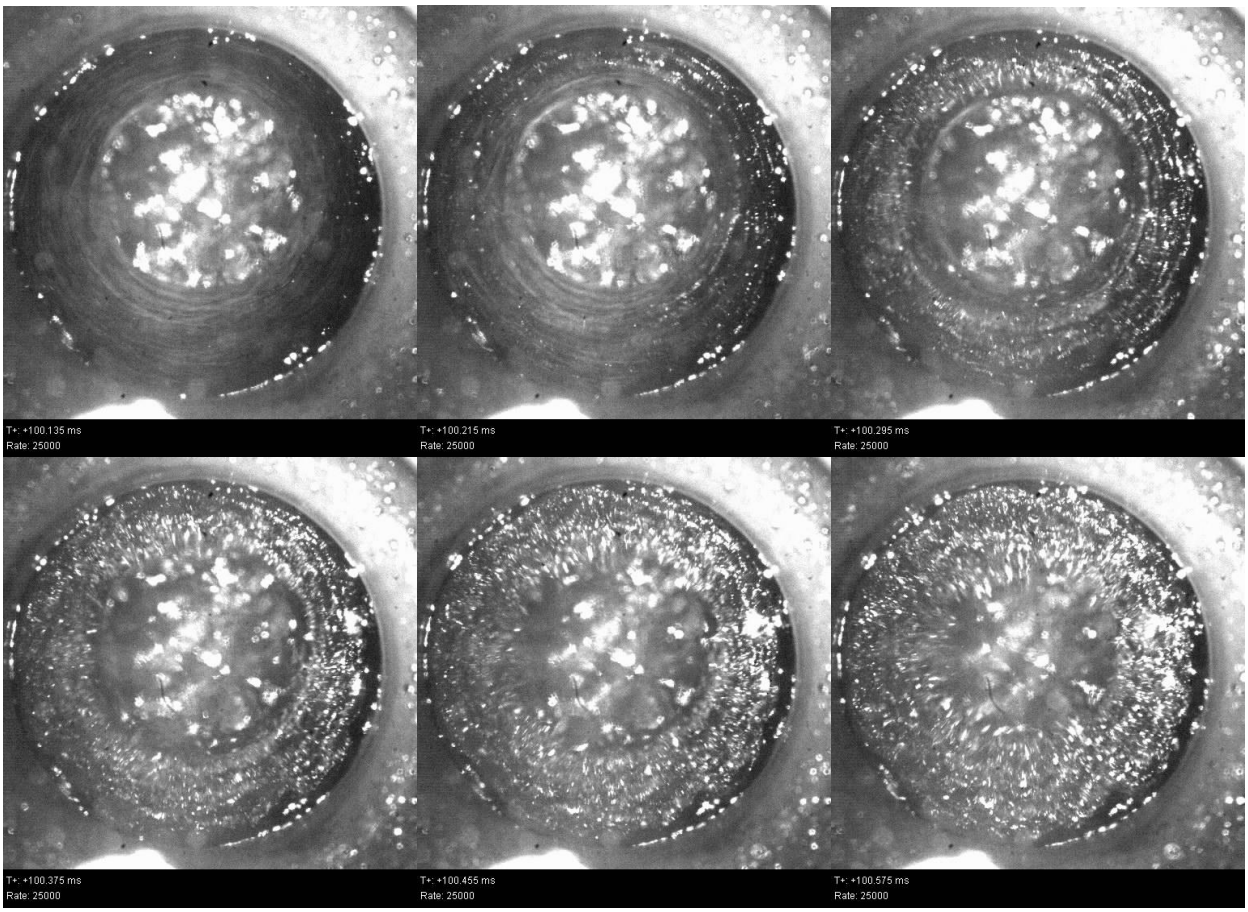

Figure 6: Vortex collapse from 7 m/s impact of 14 pistons filmed at 25,000 FPS. This sequence shows the first 480us of the collapse, divided into 80 us frames. View is looking down the axis of a ~10 cm dia vertically oriented vortex. The timing results were excellent for this 7 m/s shot, with a total arrival timing spread of: +48/-34 us.

2.1 Cavity collapse simulations

Extensive computational fluid dynamics (CFD) and finite element analysis (FEA) using LS-Dyna or Ansys Explicit STR FEA software been performed to design the Mini-Sphere (Figure 6). Models were made to predict pressure wave propagation and the shape of vortex collapse by testing different piston impact velocities, impact timings, piston positions, and reactor shapes. Due to the small size of the Mini-Sphere, the 14 pistons are expected to compress the vortex from the center towards the poles. Simulations have shown that compression from the poles to the center on a larger system can be accomplished by timing the piston impacts to create an oblate spheroidal wave front.

Identifying and reducing potential damage to the Mini-sphere and its auxiliary systems is an important role of modeling. For example, estimations of "Water hammer" behaviour in the Mini-Sphere have indicated that the pressure wave initiated by the pistons will enter the pumping system (Figure 7). Methods for mitigating damage to the pipes and Pb pumps are being investigated and simulated to calculate the forces on the supporting structure resulting from asymmetric firing of the 14 pistons.

With the Mini-Sphere and the Mini-Piston fully operational, extensive numerical simulations have been carried out to improve the understanding of the various phenomena involved in the processes. The main focus has been on exploring different factors affecting the quality of the lead shell surface as it collapses the cavity. It is well-known that interaction between pressure wave and free surface originates development of Richtmyer-Meshkov [8,9] instability that may potentially affect the efficiency of the plasma compression. Thus the ability to predict reliably a threshold for the acceptable level of initial perturbations (i.e. imperfection of the vortex surface, timing of the pistons, non-uniformity of Pb etc.) is very important. Effects of geometrical convergence, perturbation amplitude, perturbation mode, asymmetry of the imploding wave and rotation were thoroughly studied numerically using previously developed models and validated against existing numerical and experimental results where possible.

Typical results are shown in Figures 7 and 8. Figure 7 emphasises the effect of wave asymmetry on the collapse of initially perturbed cylindrical air cavity, while figure 8 demonstrates effect of geometrical convergence (compare figure 7 and figure 8 for cylindrical and planar geometries with similar initial perturbation and pressure pulse).

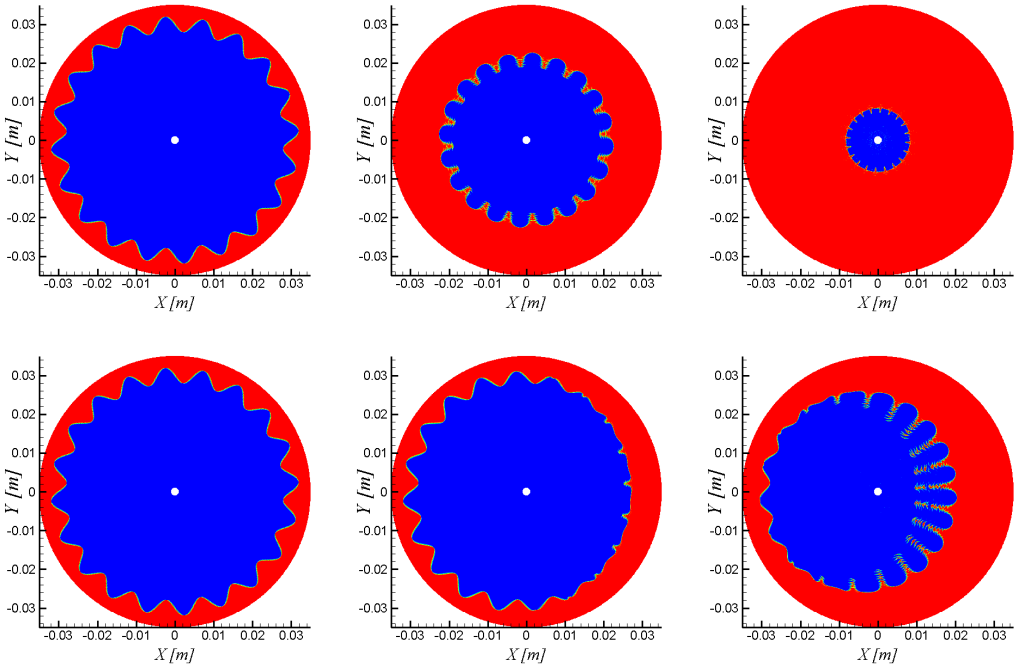

Fig. 7: Effect of the asymmetry of the imploding wave. First row shows collapse of the initially perturbed air cavity by perfectly symmetric imploding cylindrical pressure wave. Second row shows collapse of exactly the same cavity when the pressure wave is generated by a single piston (pressure wave arrives from the right). Difference in the perturbation growth is due to different geometrical convergence experienced by the air-cavity during the collapse for the results shown in rows one and two. Simulations were performed on the set of parameters relevant to Mini - Sphere using OpenFOAM CFD software.

For the hydrodynamic simulations General Fusion uses OpenFOAM CFD software while the input is frequently provided by FSI and structural simulations performed with LS-Dyna or Ansys Explicit STR FEA software.

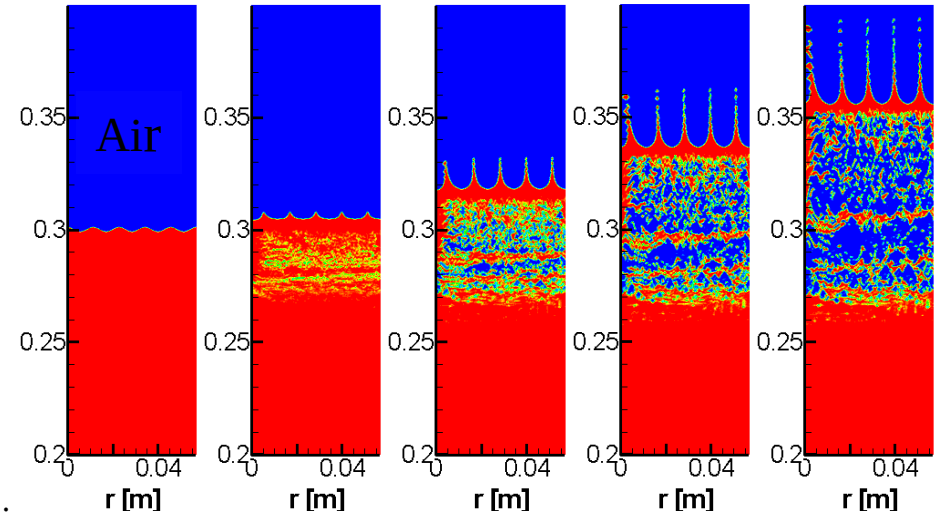

Figure 8: Effect of initial free surface imperfection on the characteristics of the detached Pb layer formed as a result of interaction between pressure pulse and free surface (Pressure wave travels from Pb into air). Spiky structures propagating into the air are due to Richtmyer-Meshkov instability developing after the pressure pulse hits the interface. Simulations are carried out in a planar geometry on a set of parameters corresponding to mini piston experiments.

3. Progress on Plasma Injector

General Fusion has two types of plasma injectors, a small direct formation device (MRT) and larger more energetic devices (PI1 and PI2). A schematic of the small injector is shown in Figure 9 (a) and the two large injectors are pictured in Figure 9 (b). The second large injector was constructed and commissioned in 2012. The large devices have both a formation section and an accelerations section. The various steps involved in creating and compressing a CT in the large plasma injector are shown in Figure 10.

The goal of the large injector is to have a magnetic and temperature life in the pot of greater than 100 microseconds. In mid-2012 General Fusion believed this had been achieved. The early part of the year was marked with good acceleration performance and in June GF achieved good separation of the CT in the injector's flux conserver from the accelerator section as shown in Figure 10 clear showing a magnetic lifetime > 100 microseconds. Unfortunately a few days later it was determined that the temperature as measured by Thomson Scattering was falling off in ~30 microseconds. Several months of testing revealed that the primary cause of the cooling was loss of heat confinement due to poorly formed and maintained flux surfaces.

Careful investigation of the possible input parameter space coupled with improvements in computer simulation resulted in greatly improved heat confinement in formation. Confinement improved to the point that compression heating via contraction of the CT and/or ohmic heating of the plasma was observed during formation. This result is shown in Figure 12. Heating continued for ~200 microseconds until the magnetic surfaces crossed through an instability resulting in distortions in the flux surfaces and loss of confinement.

Subsequent acceleration of the well-formed CT indicated adiabatic heating of the CT in compression. A CT formed at location 118 cm with 0.2 T, 40 eV, and 0.5e+14 cm^{-3} when accelerated had 0.8 T, 160 eV, 4.0e+14 cm^{-3} at location 352 (2x radial compression) and 3.0 T, 640 eV, and 3.0e+15 at location 493 (further 2x radial compression). Note the 640 eV temperature is uncertain because it has not yet been possible to verify it with Thomson Scattering as the signal is lost at that temperature and density.

General Fusion has continued to made progress in forming and accelerating compact toroids (CT) and is nearing the requirements for long lasting, stable, and hot CTs in the target chamber. A series of design changes were implemented and tested, eventually resulting in good formation and acceleration of CTs. The acceleration current now delivers most of its energy into acceleration, allowing it to reach elevated temperatures and magnetic fields. Formation efficiency is ~45% and acceleration efficiency is ~ 20% (energy in CT/discharge energy from relevant capacitor bank).

Performance achieved to date on both types of injectors is summarized in the following table.

Device	**Plasma type**	**Temp eV**	**Temp Time µs**	**Density cm^{-3}**	**B Field T**
MRT	He	30	70	1.0e+16	1.5
MRT	D	75	100	2.0e+15	1.2
PI1 formation	D	100	200	1.0e+14	0.4
PI1 @ 352	D	160	n/a	1.0e+15	0.8
PI1 @ 493	D	>250	n/a	4.0e+16	3.0

Table 1: Comparison of plasma parameters GF has achieved to date on two types of plasma injectors using either helium or deuterium.

All temperatures have been measured with Thomson Scattering which is General Fusion's standard temperature method. Ion Doppler, X-ray photodiodes, and neutronics are also used but each of these are line averages, vary during time (in the case of Ion Doppler, ion species become full ionized), or bulk measurements. This can result in errors and uncertainty due to plasma turbulence.

3.1 Computer Simulation of Plasma

Computer simulation of plasma at General Fusion is essential to understand the complex physics of the machines. The primary simulation tool is the Versatile Advection Code (VAC) [10], which is a shock-capturing magnetohydrodynamics (MHD) code. The version used was augmented at General Fusion to include coupling to lumped circuits (the formation and acceleration capacitor banks) and additional physics like radiative cooling, plasma viscosity, etc. Other codes were developed in-house, for example to simulate compression of plasma to fusion conditions. As well as improving the simulations themselves, General Fusion also introduced more powerful techniques for analyzing simulation results, such as the safety factor profile, mode structure (Figure 13a), and magnetic surface stochasticity (Figure 13b).

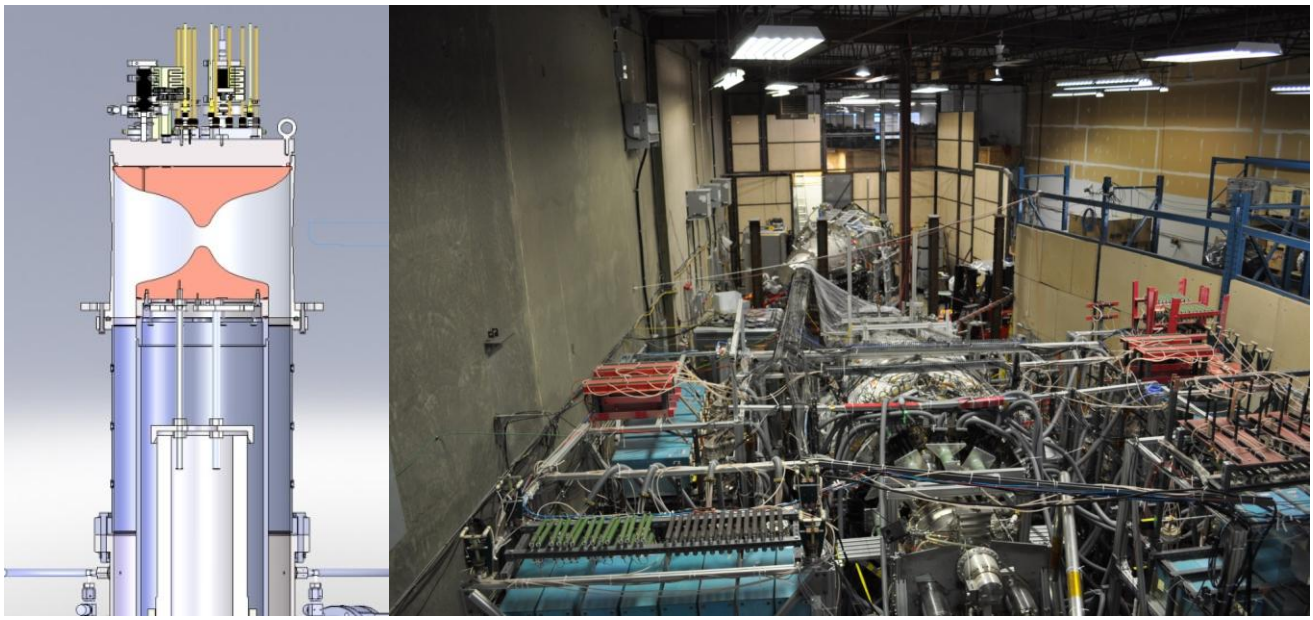

(a) **(b)**

Figure 9: (a) Schematic of small plasma injector named MRT, diameter of injector is 30 cm. (b) Picture of large plasma injectors PI1 and PI2. PI1 and PI2 are designed and located to face each other for eventual CT merging experiments.

Work focused on simulating the ongoing plasma injector (PI) and magnetized ring test (MRT) experiments. In the PI work the simulation provided valuable insights into the operation of the injector, leading to a number of design improvements. In the MRT work GF introduced the use of a finite-element code (FEMM) to calculate magnetic field profiles in the presence of iron components (Figure 14a). These profiles are part of the initial conditions required to begin a MHD simulation (Figure 14b).

GF advanced the use of 3-D simulations to reveal behavior that cannot be captured by 2-D (axially symmetric) simulations. For example, a model of the gas puff valves predicts a certain level of mass loading asymmetry and 3-D simulation shows how this can affect CT formation in the plasma injector. Asymmetric magnetic signals predicted by simulation were similar to those being observed in reality.

Other work addressed future design improvements and experiments. Simulations of the planned experiment to merge spheromaks from a pair of opposing plasma injectors reveal that large halo currents may form (Figure 15). As these currents may vaporize material from the wall, it is important to determine how to minimize them.

At the beginning of 2013 the following work is underway: improve the plasma thermal conduction model by addition of field-line following algorithm to VAC, generalize VAC to handle multi-block geometry, introduce the fusion-community CORSICA [11] code for generation of plasma equilibria for simulation as well as for fitting of experimental data.

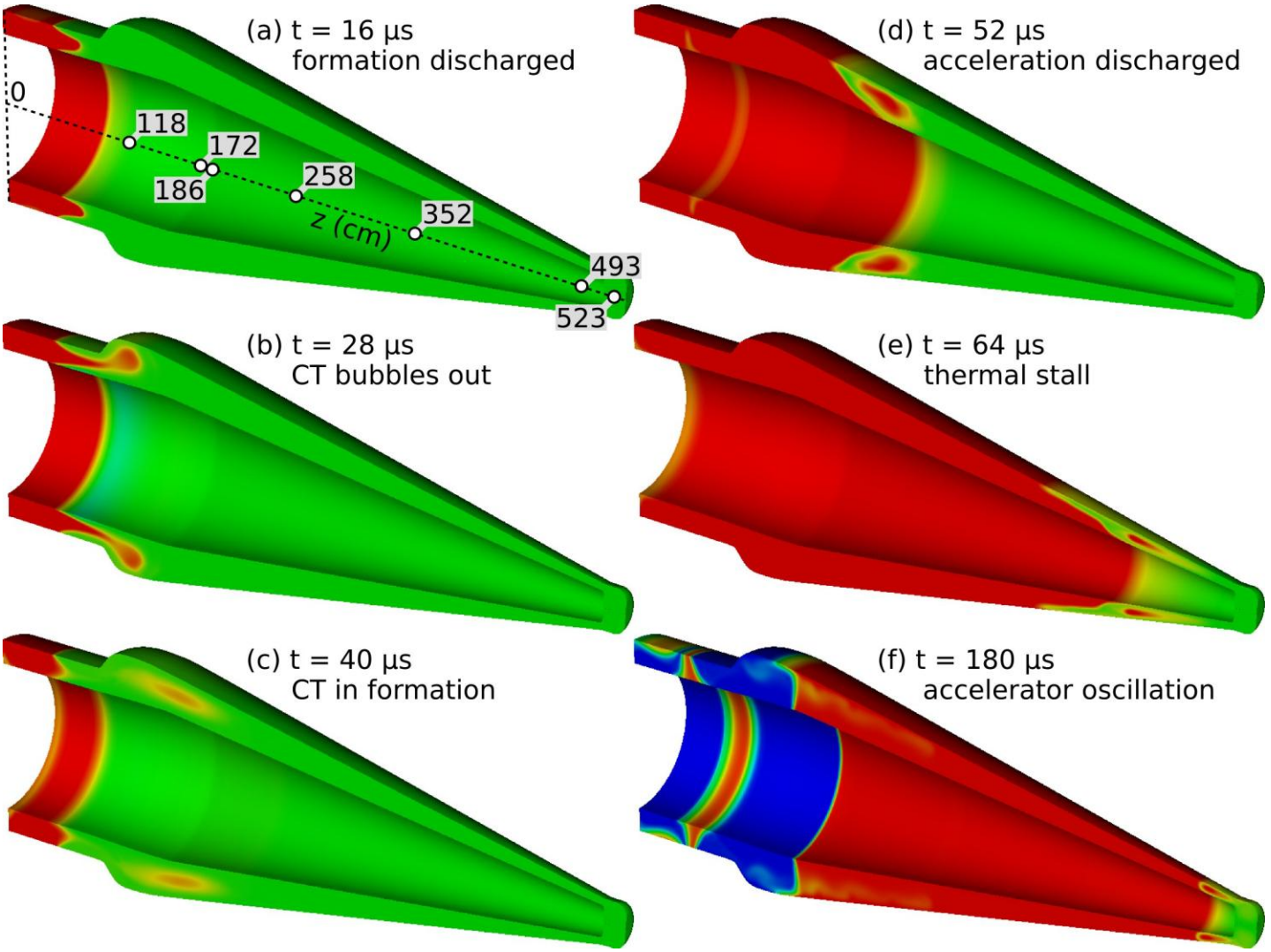

Figure 10: Simulation of poloidal current in the plasma injector done with VAC (red positive, blue negative). Axial positions of probe ports are marked by white circles in (a). The plots show the poloidal current as calculated in an axisymmetric magnetohydrodynamic simulation done with VAC, (Versatile Advection Code). (a) Initially, a voltage is applied to the formation electrode, which increases the toroidal magnetic field in the formation region. (b) The toroidal field interacts with the poloidal stuffing field to bubble out a CT. (c) The CT separates from the stuffing field and sits in the formation region. (d) A voltage is then applied to the acceleration electrode, increasing the toroidal field behind the CT and pushing the CT down the injector. (e) Sometimes the thermal pressure in the CT becomes larger than the pushing force applied by the acceleration current, causing it to slow down. (f) The energy capacitors and injector are analogous to an LRC circuit, so the accelerator voltage oscillates after pushing the CT to the target chamber.

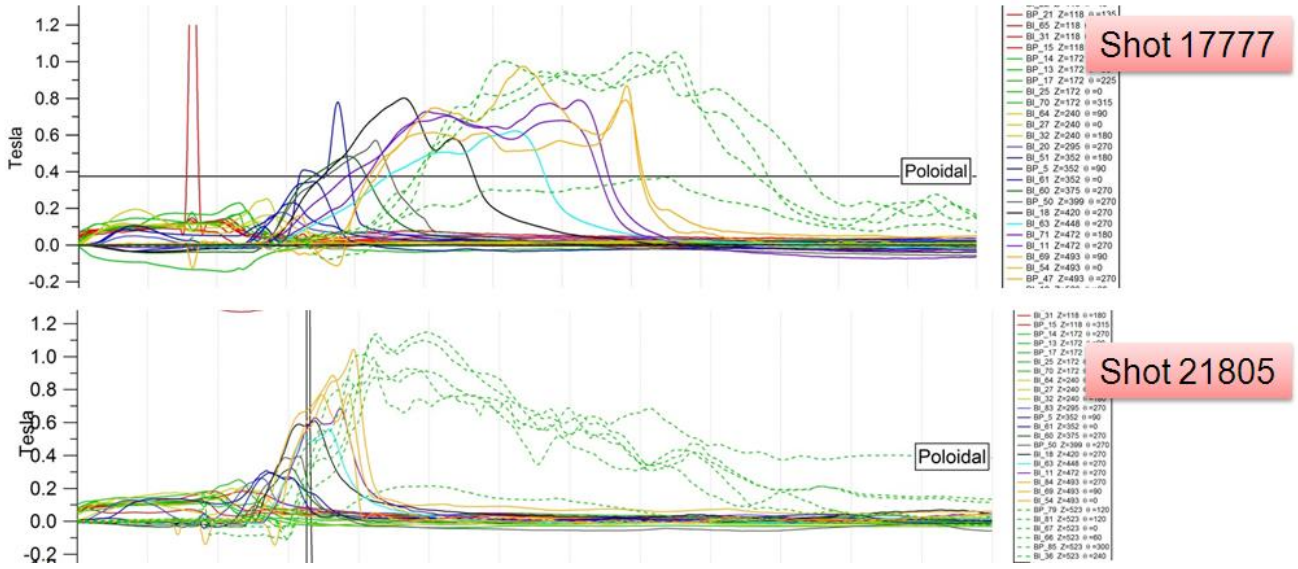

Figure 11: Plots of injector magnetic field displaying "pot" magnetic field separated from accelerator magnetic field. Shot 17777 only lasts 30 µs past the 493 position (yellow lines) while 21805 has 80 µs past the 493 position. Shots like 21805 were accompanied by hot temperature measurements from both ion Doppler and X-ray techniques.

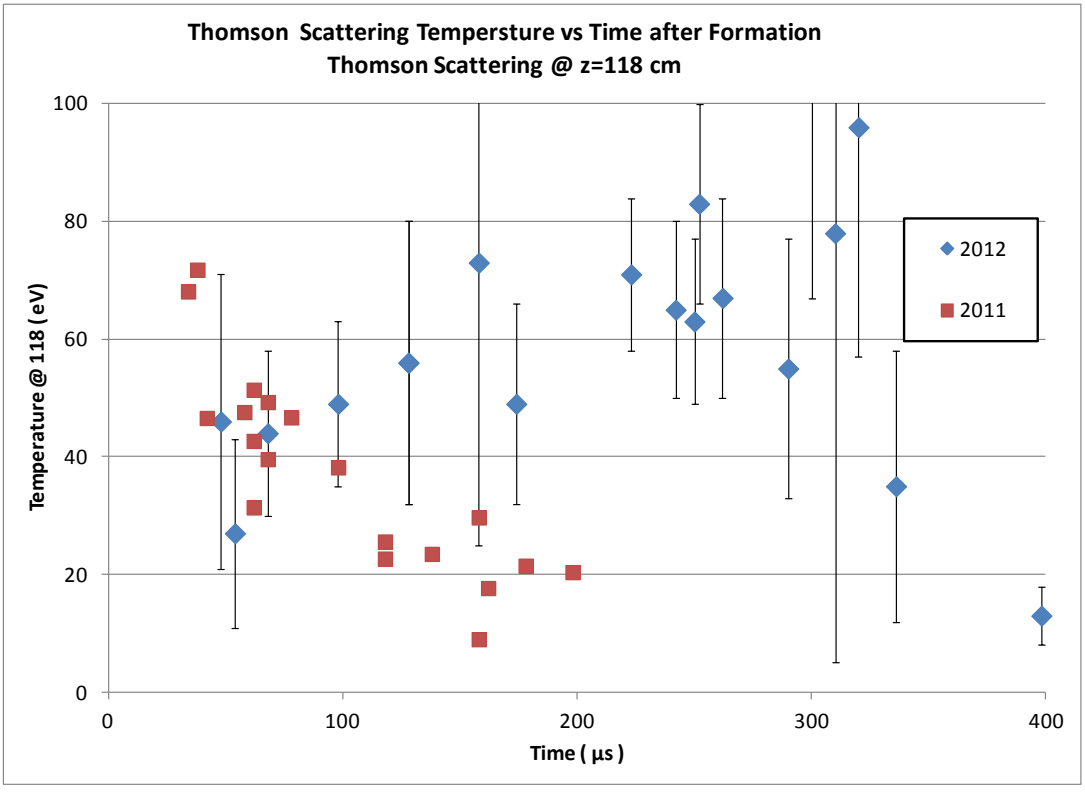

Figure 12: Composite time history shows that in 2011 the CT is formed at temperatures well above 50 eV and then quickly cools which is compared with 2012 data showing CT heating and good heat confinement consistent with closed flux surfaces.

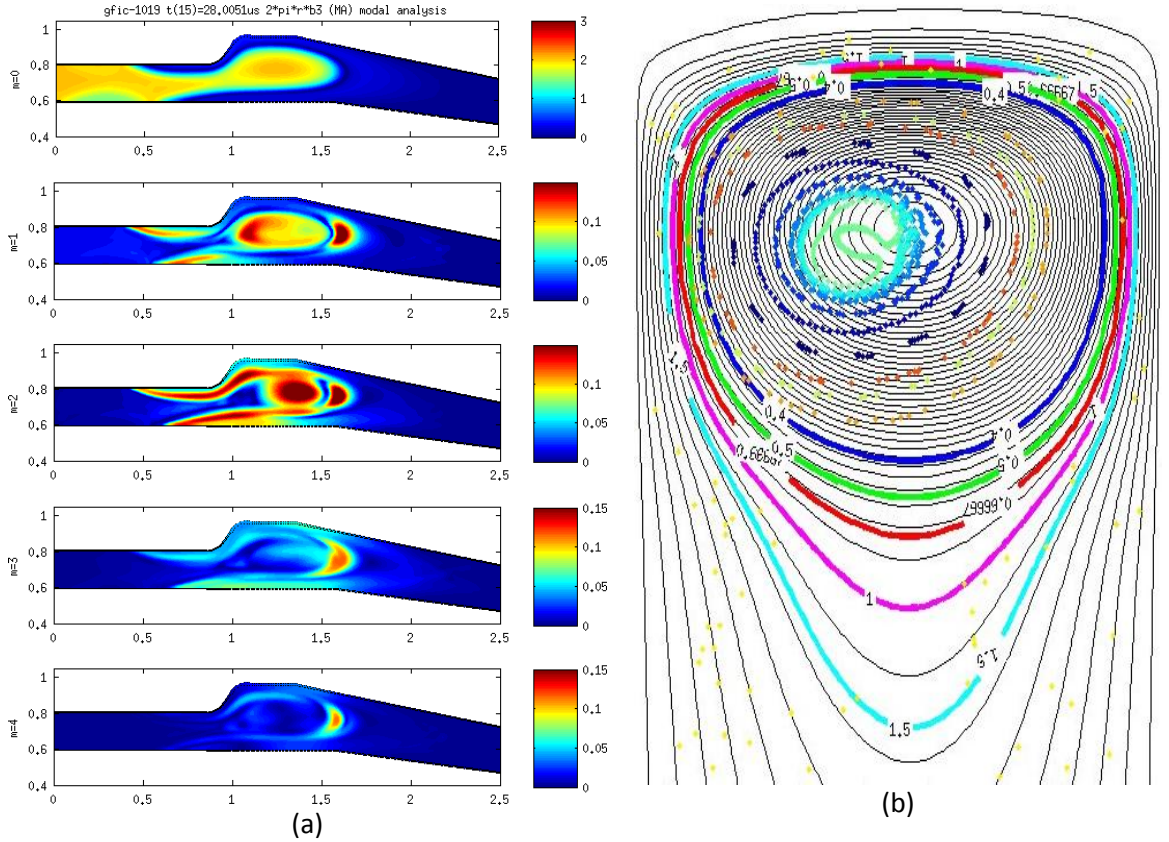

Figure 13: (a) Toroidal mode structure of a CT that has bubbled-out in a plasma injector. Top plot is axisymmetric component, 2nd through 5th plots show contribution of modes 1 through 4. (b) Poincare plot of magnetic field in CT undergoing acceleration. The flux surfaces can become helical without loss of confinement. Each dot colour is a distinct magnetic field line. The solid lines indicate rational q surfaces.

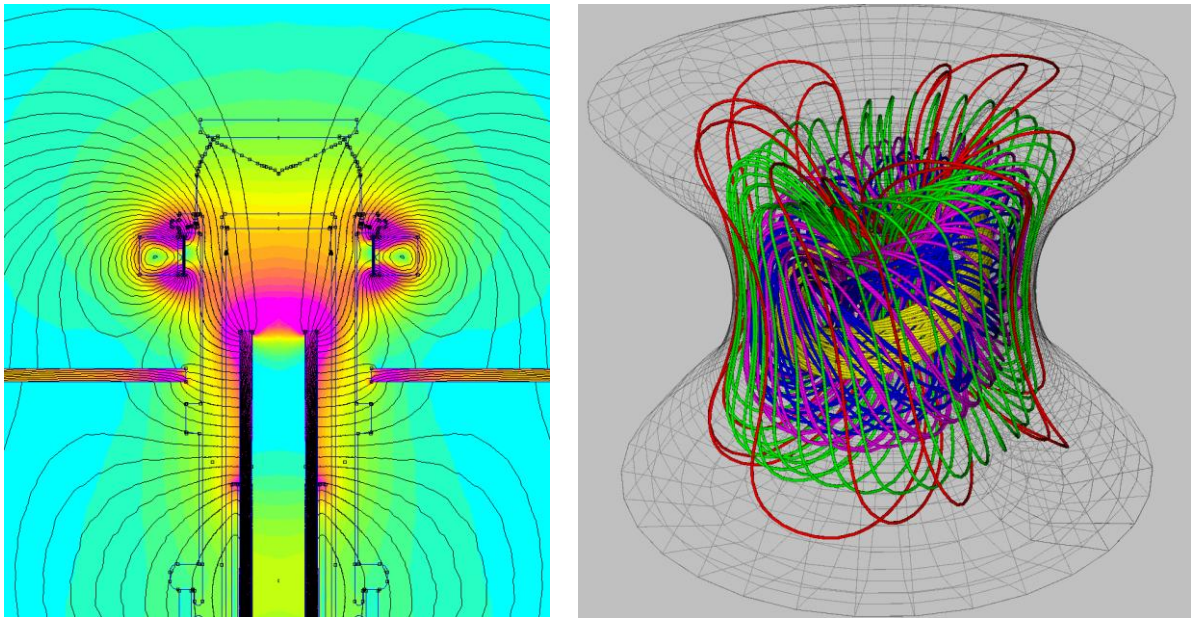

Figure 14: (a) Initial magnetic field configuration for MRT device as calculated by FEMM. Black lines show poloidal flux contours and colours show magnetic field strength (cyan low, magenta high). (b) Trace of magnetic field lines inside MRT pot as it is compressed by a shaped pinch.

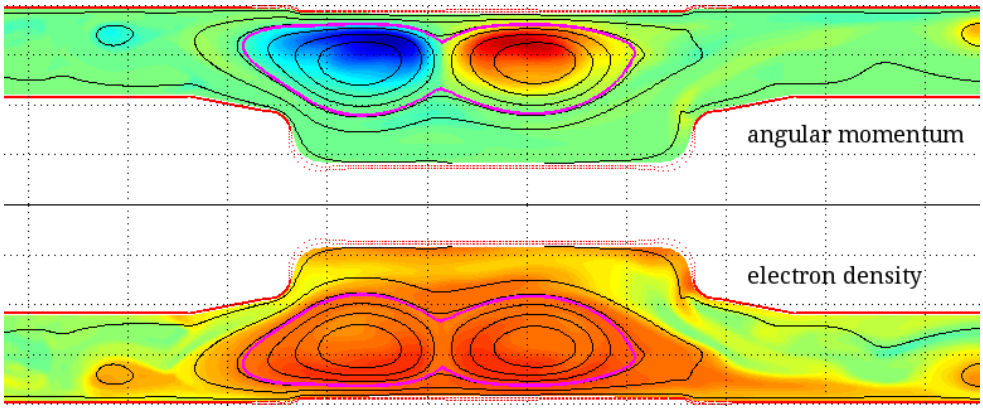

Figure 15: Two spheromaks of opposite helicity meeting in a drift tube with an inward expansion region. Top plot is coloured by angular momentum and bottom by electron density. Black lines show poloidal flux contours.

4. Summary

The previous year has seen much progress towards creating and compressing plasma and the outlook is now very encouraging. In particular, plasma densities of 10^{16} ions/cm^3 at >250 eV electron temperatures and up to 500 eV plasma ion temperatures have been demonstrated. Indications are that the formation region of the injector has achieved closed flux surfaces and that these surfaces are maintained during acceleration allowing for adiabatic compression and heating. Piston impact speeds of 50 m/s and servo-controlled impact timing accurate to ±2 µs have been achieved. The 14-piston liquid Pb Mini-Sphere assembly for testing vortex generation and piston impact has been fully commissioned and is collecting data.

General Fusion is buoyed by recent progress on all fronts of the MTF program. Improvements in piston survival, liquid Pb handling, plasma temperature, acceleration efficiency, injector reliability, and regulatory matters have left the team and investors with a positive outlook on the coming year and the company's ability to meet goals.

5. Acknowledgements

The authors would like to acknowledge the work of the entire General Fusion team for their ongoing efforts in the development of this technology. General Fusion is funded by private investors including Chrysalix Energy Ventures, Growthworks, Business Development Bank of Canada, Braemar Energy Ventures, Entrepreneurs Fund, SET Ventures, Bezos Expeditions, and Cenovus Energy. General Fusion's work is also funded in part by a grant from Sustainable Development Technology Canada.

6. References

[1] J. D. Lawson, "Some Criteria for a Power Producing Thermonuclear Reactor", *Proceedings of the Physical Society. Section B*, Vol. 70, Iss. 1, 1957.

[2] R. L. Miller and R. A. Krakowski, "Assessment of the slowly-imploding liner (LINUS) fusion reactor concept", 4th ANS Topical Meeting on the Technology of Controlled Nuclear Fusion, 1980 October 14-17.

[3] R. Siemon, I Lindemuth, K. Schoenberg, "Why Magnetized Target Fusion Offers A Low-Cost Development Path for Fusion Energy", Comments on Plasma Physics and Controlled Fusion, 1997.

[4] R. Siemon *et al.,* "The relevance of Magnetized Target Fusion (MTF) to practical energy production, a white paper for the Fusion Energy Sciences Advisory Committee", *Los Alamos National Labs,* 1999, http://fusionenergy.lanl.gov/Documents/MTF/MTF_Appl._whitepaper_6-99.PDF

[5] D. Dudzick, "Nucleonic aspects of the LINUS imploding blanket", ANS Meeting on the Technology of Controlled Thermonuclear Fusion, Santa Fe, New Mexico, USA, 1978 May 9.

[6] M. E. Sawan, M. A. Abdou, "Physics and technology conditions for attaining tritium self-sufficiency for the DT fuel cycle", *Fusion Engineering and Design*, Vol. 81, 2006, pp. 1131-1144.

[7] M. Moyer, "Fusion's False Dawn", *Scientific American*, March, 2010**,** pp. 50-57.

[8] R. D. Richtmyer, Taylor instability in shock acceleration of compressible fluids, Commun. Pure Appl. Math. 13(1960) 297–319.

[9] E. E. Meshkov, Instability of the interface of two gases accelerated by a shock wave, Fluid Dyn. 4(5) (1969) 101–104.

[10] Toth G., 1996, Astrophys. Lett. & Comm. 34, 245

[11] Crotinger J A et al 1997 LLNL Report UCRL-ID-126284; NTIS #PB2005-102154.